Available online at www.sciencedirect.com

ScienceDirect

Nuclear Physics B 966 (2021) 115387

NUCLEAR PHYSICS B

www.elsevier.com/locate/nuclphysb

Pion generalized parton distributions and light-front wave functions in the Nambu–Jona-Lasinio model

Jin-Li Zhang [a,*], Meng-Yun Lai [b], Hong-Shi Zong [c], Jia-Lun Ping [a,*]

[a] *Department of Physics, Nanjing Normal University, Nanjing 210023, China*
[b] *College of Physics and Communication Electronics Jiangxi Normal University Nanchang Jiangxi 330022, China*
[c] *Department of Physics, Nanjing University, Nanjing 210093, China*

Received 15 January 2021; received in revised form 21 March 2021; accepted 23 March 2021
Available online 26 March 2021
Editor: Hong-Jian He

Abstract

Pion generalized parton distributions and light-front wave functions are investigated in the framework of Nambu–Jona-Lasinio model. The properties of pion generalized parton distributions and light-front wave functions are examined separately. Proceeding from generalized parton distributions and light-front wave functions to form factors, parton distribution functions, parton distribution amplitudes and transverse momentum dependent parton distributions, giving a complete picture of pion structure. Moreover, comparing these distributions from the two different methods and examining their peculiarities, finding that the two methods give the same distributions. This means that generalized parton distributions and light-front wave functions give the same multi-dimensional mapping of pion in the Nambu–Jona-Lasinio model. In addition, we studied generalized form factors of pion: the quark pressure distribution θ_1 and the quark mass distribution θ_2, both are harder than electromagnetic form factor. The tensor anomalous magnetic moment $B_{1,0}$ and the tensor generalized form factor $B_{2,0}$ are harder than corresponding lattice data.

1. Introduction

One of the main open questions of strong interaction is how the nucleon and hadrons are composed of the fundamental degrees of freedom of Quantum Chromodynamics (QCD), quarks

* Corresponding authors.
E-mail addresses: jlzhang@njnu.edu.cn (J.-L. Zhang), jlping@njnu.edu.cn (J.-L. Ping).

https://doi.org/10.1016/j.nuclphysb.2021.115387

and gluons. Hard reactions can provide important information of the hadron structure [1], one of the most important hard process is deeply virtual Compton scattering (DVCS), which can be expressed in terms of the so-called generalized parton distributions (GPDs) [2–8] in the asymptotic regime. GPDs provide more than the ordinary parton distribution functions (PDFs) [9–12] and form factors (FFs) [13,14] in understanding the dynamical information of the hadron internal structure. Actually, FFs and PDFs provide the spatial and momentum quark distributions in hadrons in a separate way, respectively. GPDs stem from hadronic matrix elements that are nondiagonal with respect to hadron states and involve quark and gluon operators separated by lightlike distance [15]. Thus provide a simultaneous phase-space description of hadron as far as the position momentum uncertainty relation permits [16,17]. Due to the nondiagonal property of the matrix, GPDs not only depend on the longitudinal momentum fraction x, but also the skewness parameter ξ and square of the momentum transfer q^2 between the initial and final hadron. When taking a two-dimensional Fourier transform of GPDs at $\xi = 0$, one can get impact parameter dependent parton distributions [18,19]. Impact parameter dependent parton distributions contain information of how partons are distributed in the plane transverse to hadron moving direction. Thus give us information of the helicity carried by partons or gluons.

It is hard to calculate GPDs from QCD directly, so effective models have been used to provide estimates for experiments. People can build realistic models for GPDs by fixing their parameters through experiment data, too. One crucial point for the model building is that, in specific limits, GPDs can reduce to more familiar functions that can describe the hadronic structure, such as PDFs and FFs. The reduction relations between GPDs and these functions can serve as a test for building phenomenological models of GPDs.

Light-front wave functions (LFWFs) connecting hadrons to their composition at quark and gluon degrees of freedom. So LFWFs can describe a wide range of hadronic and nuclear physics phenomena [20]. There exists a simple decomposition of these matrix elements in terms of the light-cone Fock space wave functions of the initial and final states [21]. So a fruitful idea in the model building is to construct GPDs from LFWFs [22,23]. This representation of GPDs is ideal for physical intuition; however, comparatively little has been done to show that LFWFs representation is consistent with the reduction properties of GPDs [24]. In addition to GPDs, many hadronic observables can be computed from LFWFs, such as FFs, PDFs, transverse momentum dependent parton distributions (TMDs) and parton distribution amplitudes (PDAs) [25]. The determination of hadron LFWFs from phenomenological constraints and from QCD itself is a central goal of hadron and nuclear physics. In principle, one can solve for the hadronic LFWFs directly from fundamental theory using nonperturbative methods, such as discretized light-front quantization, the transverse lattice, lattice gauge theory moments, or Dyson-Schwinger techniques.

As a first step, in this paper, we investigate pion GPDs and LFWFs in the Nambu–Jona-Lasinio (NJL) [26–31] model. NJL model has an effective Lagrangian of relativistic fermions interacting through local fermion-fermion couplings, and especially, it preserves one of the most important fundamental symmetries of QCD, namely, chiral symmetry, which is essential in the understanding of the lightest hadron.

This paper is organized as follows: In Sec. 2, first, a brief introduction to the NJL model. Then the definition and calculation of pion GPDs in this model, in addition, basic properties of GPDs have been examined. In Sec. 3, pion LFWFs have been discussed, the relationship of LFWFs with pion PDFs, FFs, PDAs and GPDs will be given. A brief summary and discussion are given in Sec. 4.

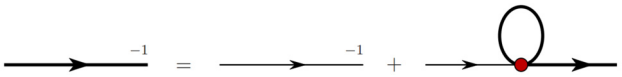

Fig. 1. The NJL gap equation in the Hartree-Fock approximation, where the thin line represents the elementary quark propagator, the shaded circle represents the $\bar{q}q$ interaction kernel. Higher-order terms, attributed to meson loops for example, are not included in the gap equation kernel.

2. Generalized parton distributions

GPDs contain a mass of inaccessible information about hadron structure and have been under deep theoretical and experimental studies. In this section, we calculate pion vector and tensor GPDs in the NJL model and check their properties.

2.1. Nambu–Jona-Lasinio model

NJL has an effective Lagrangian of relativistic fermions interacting through 4-fermions contact interaction. It might serve as a suitable approximation to QCD in the low-energy and long-wavelength limit, assuming that gluon degrees of freedom can be frozen into effective point-like interactions between quarks. A prominent feature of the model is that it is a Poincaré covariant quantum field theory where interactions dynamically break chiral symmetry, giving rise to dynamically generated dressed quark masses, pion is a $\bar{q}q$ bound state with the properties of a pseudo-Goldstone boson and a large mass splitting between low-lying chiral partners. Generally, NJL results are to be identified as qualitatively sound initial conditions for use in exploring the domain of physical possibilities in areas where more realistic frameworks are not yet able to provide insights or predictions, so that is widely used in many fields. NJL model has a long history of success in the study of meson properties [13,32], baryon properties [33,34], nucleon PDFs [35,36], electromagnetic FFs [37], quark fragmentation functions [38,39] and TMDs [40].

The SU(2) flavor NJL Lagrangian, in the $q\bar{q}$ interaction channel, reads

$$\begin{aligned}\mathcal{L} = &\bar{\psi}\left(i\gamma^{\mu}\partial_{\mu} - \hat{m}\right)\psi + \frac{1}{2}G_{\pi}[\left(\bar{\psi}\psi\right)^2 - \left(\bar{\psi}\gamma_5\vec{\tau}\psi\right)^2] - \frac{1}{2}G_{\omega}\left(\bar{\psi}\gamma_{\mu}\psi\right)^2 \\ &- \frac{1}{2}G_{\rho}[\left(\bar{\psi}\gamma_{\mu}\vec{\tau}\psi\right)^2 + \left(\bar{\psi}\gamma_{\mu}\gamma_5\vec{\tau}\psi\right)^2],\end{aligned} \tag{1}$$

where $\vec{\tau}$ are the Pauli matrices representing isospin and $\hat{m} \equiv \mathrm{diag}\,[m_u, m_d]$ is current quark mass matrix. When working in the limit of exact isospin symmetry, $m_u = m_d = m$. The 4-fermion coupling constants in each chiral channel are labeled by G_{π}, G_{ω}, and G_{ρ}.

The elementary quark-antiquark interaction kernel is defined as

$$\begin{aligned}\mathcal{K}_{\alpha\beta,\gamma\delta} &= \sum_{\Omega} K_{\Omega}\Omega_{\alpha\beta}\bar{\Omega}_{\gamma\delta} \\ &= 2iG_{\pi}[(\mathbb{1})_{\alpha\beta}(\mathbb{1})_{\gamma\delta} - (\gamma_5\tau_i)_{\alpha\beta}(\gamma_5\tau_i)_{\gamma\delta}] \\ &- 2iG_{\rho}[(\gamma_{\mu}\tau_i)_{\alpha\beta}(\gamma_{\mu}\tau_i)_{\gamma\delta} + (\gamma_{\mu}\gamma_5\tau_i)_{\alpha\beta}(\gamma_{\mu}\gamma_5\tau_i)_{\gamma\delta}] \\ &- 2iG_{\omega}(\gamma_{\mu})_{\alpha\beta}(\gamma_{\mu})_{\gamma\delta},\end{aligned} \tag{2}$$

where the indices label Dirac, color, and isospin.

The dressed quark propagator of NJL model is obtained by solving the gap equation, which is illustrated in Fig. 1,

Table 1
Parameter set used in our work. The dressed quark mass and regularization parameters are in units of GeV, while coupling constant is in units of GeV^{-2}.

Λ_{IR}	Λ_{UV}	M	G_π	Z_π	m_π	G_ω	G_ρ
0.240	0.645	0.4	19.0	17.85	0.14	10.4	11.0

$$iS^{-1}(k) = iS_0^{-1}(k) - \sum_{\Omega} K_\Omega \Omega \int \frac{d^4l}{(2\pi)^4} \mathrm{tr}[\bar{\Omega} i S(l)], \tag{3}$$

where $S_0^{-1}(k) = \not{k} - m + i\varepsilon$ is the bare quark propagator and the trace is over Dirac, color, and isospin indices. The solution of gap equation is

$$S(k) = \frac{1}{\not{k} - M + i\varepsilon}. \tag{4}$$

The interaction kernel of gap equation in Fig. 1 is local, so we get a constant dressed quark mass

$$M = m + 12 i G_\pi \int \frac{d^4l}{(2\pi)^4} \mathrm{tr}_{\mathrm{D}}[S(l)], \tag{5}$$

where the trace is over Dirac indices. Only for sufficiently strong coupling $G_\pi > G_{critical}$, dynamical chiral symmetry breaking can happen, which gives a nontrivial solution $M > 0$ even in the chiral limit ($m = 0$).

NJL model is a non-renormalizable quantum field theory, an regularization method must be applied to fully define the model. We will use the proper time regularization (PTR) scheme [41, 42].

$$\frac{1}{X^n} = \frac{1}{(n-1)!} \int_0^\infty d\tau \tau^{n-1} e^{-\tau X} \to \frac{1}{(n-1)!} \int_{1/\Lambda_{\mathrm{UV}}^2}^{1/\Lambda_{\mathrm{IR}}^2} d\tau \tau^{n-1} e^{-\tau X}, \tag{6}$$

where X represents a product of propagators that have been combined using Feynman parametrization. In addition to the ultraviolet cutoff, Λ_{UV}, we also include the infrared cutoff Λ_{IR}. NJL model doesn't contain confinement, the infrared cutoff is used to mimic confinement, therefore should be of the order Λ_{QCD} and we choose $\Lambda_{\mathrm{IR}} = 0.240$ GeV. The parameters in this work, the coupling strength G_π and Λ_{UV} are determined through the Gell-Mann–Oakes–Renner (GMOR) relation, $f_\pi^2 m_\pi^2 = -m\langle\bar{\psi}\psi\rangle$ and gap equation $M = m - 2G_\pi\langle\bar{\psi}\psi\rangle$, where $m_\pi = 0.140$ GeV is the physical mass, $f_\pi = 0.092$ GeV is the pion decay constant, the constituent quark mass $M = 0.4$ GeV, $\langle\bar{\psi}\psi\rangle$ is two-quark condensate derived from QCD sum rules. G_ω and G_ρ are determined by $m_\omega = 0.782$ GeV, $m_\rho = 0.770$ GeV through $1 + 2G_i\Pi_{VV}(-m_i^2) = 0$, $i = (\omega, \rho)$, $\Pi_{VV}(Q^2)$ is defined in Eq. (12). The parameters used in this work are given in Table 1.

In the NJL model, the quark charge operator is

$$\hat{Q} = \begin{pmatrix} e_u & 0 \\ 0 & e_d \end{pmatrix} = (\frac{1}{6} + \frac{\tau_3}{2}), \tag{7}$$

where e_u and e_d are the u and d quark charges. This means quark-photon vertex has both an isoscalar and an isovector component, so the dressed quark-photon vertex can be expressed as

$$\Lambda^\mu_{\gamma Q}(p', p) = \frac{1}{6}\Lambda^\mu_\omega(p', p) + \frac{\tau_3}{2}\Lambda^\mu_\rho(p', p), \tag{8}$$

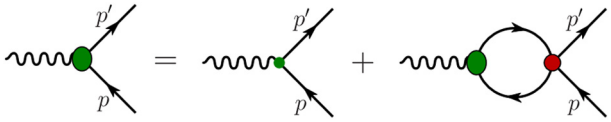

Fig. 2. Inhomogeneous BSE whose solution gives the quark-photon vertex, represented as the large shaded oval.

the effective vertex

$$\Lambda_i^\mu(Q^2) = \gamma^\mu F_{1i}(Q^2) + \frac{\sigma^{\mu\nu}q_\nu}{2M}F_{2i}(Q^2), \tag{9}$$

where $i = (\omega, \rho)$. This vertex has the same form as the electromagnetic current for an on-shell spin-$\frac{1}{2}$ fermion. For a point-like quark $F_{1i}(Q^2) = 1$ and $F_{2i}(Q^2) = 0$. The inhomogeneous Bethe-Salpeter equation (BSE) for the quark-photon vertex, described in Fig. 2, reads,

$$\begin{aligned}\Lambda^\mu_{\gamma Q}(p', p) = {} & \gamma^\mu\left(\frac{1}{6} + \frac{\tau_3}{2}\right) \\ & + \sum_\Omega K_\Omega \Omega \int \frac{d^4k}{(2\pi)^4}\mathrm{tr}[\bar{\Omega}S(k+q)\Lambda^\mu_{\gamma Q}(k+q,k)S(k)],\end{aligned} \tag{10}$$

where $\sum_\Omega K_\Omega \Omega_{\alpha\beta}\bar{\Omega}_{\gamma\delta}$ represent the interaction kernels in Eq. (2), only the isovector-vector, $-2iG_\rho(\gamma_\mu\vec{\tau})_{\alpha\beta}(\gamma_\mu\vec{\tau})_{\gamma\delta}$, and isoscalar-vector $-2iG_\omega(\gamma_\mu)_{\alpha\beta}(\gamma_\mu)_{\gamma\delta}$ terms can contribute.

From the inhomogeneous BSE, the dressed quark form factors, associated with the electromagnetic current of Eq. (9), are

$$F_{1i}(Q^2) = \frac{1}{1 + 2G_i\Pi_{VV}(Q^2)}, \qquad F_{2i}(Q^2) = 0, \tag{11}$$

where $i = (\omega, \rho)$, Π_{VV} is the bubble diagram

$$\Pi_{VV}(Q^2) = \frac{3}{\pi^2}\int_0^1 dx x(1-x)Q^2\bar{\mathcal{C}}_1(\sigma_2). \tag{12}$$

We will use the notations in Eqs. (A.1) and (A.5) in the following.

2.2. The definition and calculation of pion GPDs

The pion GPDs in the NJL model are given by diagrams illustrated in Fig. 3, where p is the incoming and p' the outgoing pion momentum, in this paper we will use the symmetry notation as Refs. [5,6], the kinematics of this process and the related quantities are defined as

$$p^2 = p'^2 = m_\pi^2, \quad t = q^2 = (p'-p)^2 = -Q^2, \tag{13}$$

$$\xi = \frac{p^+ - p'^+}{p^+ + p'^+}, \quad P = \frac{p+p'}{2}, \tag{14}$$

where ξ is the skewedness parameter, in the light-cone coordinate

$$v^\pm = (v^0 \pm v^3), \quad \mathbf{v} = (v^1, v^2), \tag{15}$$

for any four-vector, $n = (1, 0, 0, -1)$ is the light-cone four-vector, then v^+ in the light-cone coordinate can be given by

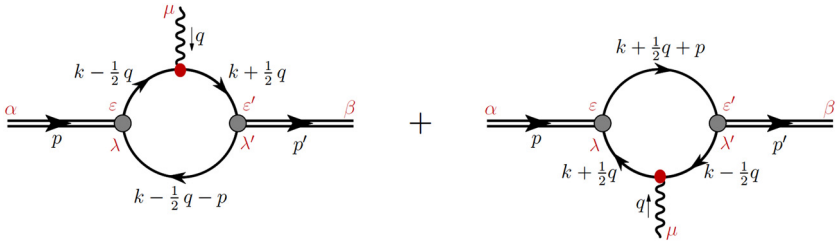

Fig. 3. Pion GPDs diagrams.

$$v^+ = v \cdot n. \tag{16}$$

These coordinates are a natural way to describe the infinite momentum frame in which parton distributions can be explained in the physical picture of parton model. The light-cone momentum p^+ will become proportional to the momentum of the particle in the infinite momentum frame $p^3 \to \infty$.

GPDs are defined through non-forward ($t \neq 0$) and nondiagonal ($\xi \neq 0$) matrix elements of quark operators at a light-like separation. The two leading-twist quark GPDs of pion are defined as

$$H(x,\xi,t) = \frac{1}{2}\int \frac{dz^-}{2\pi} e^{\frac{i}{2}x(p^+ + p'^+)z^-} \times \langle p'|\bar{q}(-\frac{1}{2}z)\gamma^+ q(\frac{1}{2}z)|p\rangle\,|_{z^+=0,z=\mathbf{0}}, \tag{17}$$

$$\frac{P^+q^j - P^jq^+}{P^+m_\pi} E(x,\xi,t) = \frac{1}{2}\int \frac{dz^-}{2\pi} e^{\frac{i}{2}x(p^+ + p'^+)z^-} \times \langle p'|\bar{q}(-\frac{1}{2}z) i\sigma^{+j} q(\frac{1}{2}z)|p\rangle\,|_{z^+=0,z=\mathbf{0}}, \tag{18}$$

where x is the longitudinal momentum fraction. The first is the vector or no spin flip GPD, the second is tensor or spin flip GPD. The operators for the two GPDs in Fig. 3 read

$$\bullet_1 = \gamma^+ \delta(x - \frac{k^+ + k'^+}{p^+ + p'^+}), \tag{19a}$$

$$\bullet_2 = i\sigma^{+j}\delta(x - \frac{k^+ + k'^+}{p^+ + p'^+}), \tag{19b}$$

$\bullet_1$ for vector GPD and $\bullet_2$ for tensor GPD. The pion vertex function, in the light-cone normalization, is given by

$$\Gamma_\pi = \sqrt{Z_\pi}\gamma_5, \tag{20}$$

where Z_π is the square of the effective meson-quark-quark coupling constant.

In the NJL model, GPDs are defined as

$$H(x,\xi,t) = 2iN_c Z_\pi \int \frac{d^4k}{(2\pi)^4}\delta_n^x(k)\mathrm{tr_D}\left[\gamma_5 S(k_{+q})\gamma^+ S(k_{-q})\gamma_5 S(k-P)\right], \tag{21}$$

$$\frac{P^+q^j - P^jq^+}{P^+m_\pi} E(x,\xi,t) = 2iN_c Z_\pi \int \frac{d^4k}{(2\pi)^4}\delta_n^x(k) \times \mathrm{tr_D}\left[\gamma_5 S(k_{+q}) i\sigma^{+j} S(k_{-q})\gamma_5 S(k-P)\right], \tag{22}$$

where $\mathrm{tr_D}$ indicates a trace over spinor indices, $\delta_n^x(k) = \delta(xP^+ - k^+)$, $k_{+q} = k + \frac{q}{2}$, $k_{-q} = k - \frac{q}{2}$. Here we use the following reduce formulae ($D(k^2) = k^2 - M^2$)

$$p \cdot q = -\frac{q^2}{2}, \tag{23a}$$

$$k \cdot q = \frac{1}{2}\left(D(k_{+q}^2) - D(k_{-q}^2)\right), \tag{23b}$$

$$k \cdot p = -\frac{1}{2}\left(D((k-P)^2) - D(k_{-q}^2) - p^2 + \frac{q^2}{2}\right), \tag{23c}$$

$$k^2 = \frac{1}{2}\left(D(k_{+q}^2) + D(k_{-q}^2)\right) + M^2 - \frac{q^2}{4}, \tag{23d}$$

applying these relationships to Eqs. (21) and (22), cancel each common numerator and denominator factor; finally use Feynman parameterizations to simplify all remaining denominators. In this way, one arrives at

$$\begin{aligned} H(x,\xi,t) = {} & \frac{N_c Z_\pi}{8\pi^2}\left[\theta_{\bar{\xi}1}\bar{\mathcal{C}}_1(\sigma_3) + \theta_{\xi 1}\bar{\mathcal{C}}_1(\sigma_4) + \theta_{\bar{\xi}\xi}\frac{x}{\xi}\bar{\mathcal{C}}_1(\sigma_5)\right] \\ & + \frac{N_c Z_\pi}{8\pi^2}\int_0^1 d\alpha \frac{\theta_{\alpha\xi}}{\xi}(2x m_\pi^2 + (1-x)t)\frac{1}{\sigma_6}\bar{\mathcal{C}}_2(\sigma_6), \end{aligned} \tag{24}$$

$$E(x,\xi,t) = \frac{N_c Z_\pi}{4\pi^2}\int_0^1 d\alpha \frac{\theta_{\alpha\xi}}{\xi} m_\pi M \frac{1}{\sigma_6}\bar{\mathcal{C}}_2(\sigma_6), \tag{25}$$

and

$$\theta_{\bar{\xi}1} = x \in [-\xi, 1], \tag{26a}$$

$$\theta_{\xi 1} = x \in [\xi, 1], \tag{26b}$$

$$\theta_{\bar{\xi}\xi} = x \in [-\xi, \xi], \tag{26c}$$

$$\theta_{\alpha\xi} = x \in [\alpha(\xi+1) - \xi, \alpha(1-\xi) + \xi] \cap x \in [-1, 1], \tag{26d}$$

where θ is the step function, x only exist in the corresponding region. One can write $\theta_{\bar{\xi}\xi}/\xi = \Theta(1 - x^2/\xi^2)$, where $\Theta(x)$ is the Heaviside function, and $\theta_{\alpha\xi}/\xi = \Theta((1-\alpha^2) - (x-\alpha)^2/\xi^2)\Theta(1-x^2)$. These results are in the region $\xi > 0$, under $\xi \to -\xi$: $\theta_{\bar{\xi}1} \leftrightarrow \theta_{\xi 1}$; and $\theta_{\bar{\xi}\xi}/\xi$, $\theta_{\alpha\xi}/\xi$ are invariant. We plot the diagrams of vector and tensor GPDs in Figs. 4 and 5. From Fig. 4 we can see in the NJL model, $H(x,\xi,0) = 0$ when $x < -\xi$, vector GPD is continuous but not differentiable at $x = \pm\xi$, tensor GPD is similar. GPDs should satisfy some basic properties, we will check these properties separately in the following section.

If we use the dressed quark photon vertex in Eq. (9) with $F_{1\rho}(Q^2)$ in Eq. (11), we can get the dressed vector and tensor GPDs.

2.3. The properties of pion GPDs

2.3.1. Forward limit

When the initial and final pion have the same momentum $p = p'$, in this case, $\xi = 0$, $t = 0$, GPDs should reduce to PDFs, we arrive at

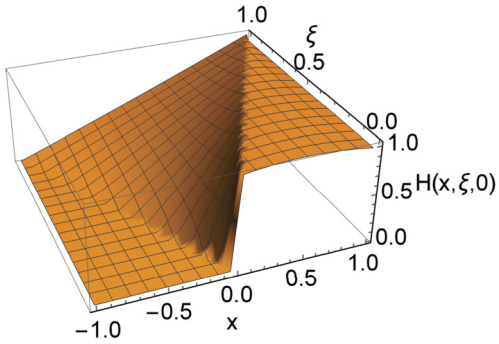

Fig. 4. Pion vector GPD $H(x,\xi,0)$, because of the symmetry property in Eq. (30), only $\xi > 0$ plotted.

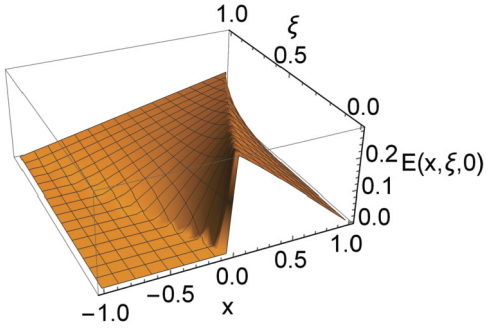

Fig. 5. Pion tensor GPD $E(x,\xi,0)$, because of the symmetry property in Eq. (31), only $\xi > 0$ plotted.

$$u(x) = \frac{3Z_\pi}{4\pi^2}\bar{\mathcal{C}}_1(\sigma_1) + \frac{3Z_\pi}{2\pi^2}x(1-x)m_\pi^2\frac{1}{\sigma_1}\bar{\mathcal{C}}_2(\sigma_1), \tag{27}$$

which satisfy

$$\int_0^1 u(x)dx = 1. \tag{28}$$

This PDF, varies around 1, only changes a little with x, this also can be seen from Fig. 4, $H(x,0,0)$ is 0 when $x \in [-1,0]$, and 1 when $x \in [0,1]$, $u(x) \approx \theta(x)\theta(1-x)$ at the pion mass $m_\pi = 0.14$ GeV, this result is similar as Eq. (7) in Ref. [43], they also work in the NJL model use Pauli-Villars procedure.

2.3.2. *Symmetry properties*

Generally speaking, GPDs are neither even nor odd of x, the combinations,

$$H^{I=0}(x,\xi,t) = H(x,\xi,t) - H(-x,\xi,t)\,, \tag{29a}$$

$$H^{I=1}(x,\xi,t) = H(x,\xi,t) + H(-x,\xi,t), \tag{29b}$$

correspond to the isoscalar (isovector) pion GPDs. The first equation corresponds to the exchange of charge conjugation $C = +1$ in the T-channel. The second equation corresponds to $C = -1$ which also called "nonsinglet" or "valence" combination, tensor GPD $E(x,\xi,t)$ is similar.

For the time reversal invariance,

$$H(x,\xi,t) = H(x,-\xi,t), \tag{30}$$
$$E(x,\xi,t) = E(x,-\xi,t), \tag{31}$$

using the results following Eqs. (26) and (A.5), we could establish that straightforward. This means our results preserve the time reversal invariance property of GPDs.

2.3.3. Polynomiality condition

Moments of the momentum fraction x play an important role in the theory of GPDs,

$$\int_{-1}^{1} x^n H(x,\xi,t)dx = \sum_{i=0}^{[(n+1)/2]} \xi^{2i} A_{n+1,2i}(t)\,, \tag{32a}$$

$$\int_{-1}^{1} x^n E(x,\xi,t)dx = \sum_{i=0}^{[(n+1)/2]} \xi^{2i} B_{n+1,2i}(t), \tag{32b}$$

where $A_{n+1,2i}(t)$ and $B_{n+1,2i}(t)$ are vector and tensor generalized factor factors (GFFs), respectively.

When $n = 0$, it is ξ independent,

$$\int_{-1}^{1} H(x,\xi,t)dx = A_{1,0}(t) = F_\pi(Q^2)\,, \tag{33a}$$

$$\int_{-1}^{1} E(x,\xi,t)dx = B_{1,0}(t) = F_\pi^T(Q^2), \tag{33b}$$

where $F_\pi(Q^2)$ and $F_\pi^T(Q^2)$ are the pion electromagnetic FF and tensor FF. $B_{1,0}(0)$ is the tensor anomalous magnetic moment for $n = 0$ [44].

$$A_{1,0}(t) = \frac{N_c Z_\pi}{4\pi^2}\int_0^1 dx\bar{\mathcal{C}}_1(\sigma_1) + \frac{N_c Z_\pi}{4\pi^2}\int_0^1 dx\int_0^{1-x} dy \times (2m_\pi^2 - (x+y)(2m_\pi^2 - t))\frac{1}{\sigma_7}\bar{\mathcal{C}}_2(\sigma_7), \tag{34}$$

$$B_{1,0}(t) = \frac{N_c Z_\pi}{2\pi^2}\int_0^1 dx\int_0^{1-x} dy\frac{Mm_\pi}{\sigma_7}\bar{\mathcal{C}}_2(\sigma_7). \tag{35}$$

For $n = 1$:

$$\int_{-1}^{1} xH(x,\xi,t)dx = A_{2,0}(t) + \xi^2 A_{2,2}(t) = \theta_2(t) - \xi^2\theta_1(t)\,, \tag{36a}$$

$$\int_{-1}^{1} xE(x,\xi,t)dx = B_{2,0}(t) + \xi^2 B_{2,2}(t), \tag{36b}$$

Table 2
GFFs at $t = 0$, $A_{2,0}(0)$, $A_{2,2}(0)$, $B_{1,0}(0)$, $B_{2,0}(0)$.

$A_{2,0}(0)$	$A_{2,2}(0)$	$B_{1,0}(0)$	$B_{2,0}(0)$
0.4999	–0.1608	0.1503	0.0503

where θ_2 relates to the quark mass distribution and θ_1 is linked to the quark pressure distribution within the pion. The GFFs are

$$A_{2,0}(t) = \frac{N_c Z_\pi}{8\pi^2}\int_0^1 dx\bar{\mathcal{C}}_1(\sigma_1) + \frac{N_c Z_\pi}{4\pi^2}\int_0^1 dx\int_0^{1-x} dy\frac{1}{\sigma_7}\bar{\mathcal{C}}_2(\sigma_7) \times (2m_\pi^2(1-x-y)^2 + t(1-x-y)(x+y)), \tag{37}$$

$$A_{2,2}(t) = -\frac{N_c Z_\pi}{4\pi^2}\int_0^1 dx(1-x)\bar{\mathcal{C}}_1(\sigma_1) - \frac{N_c Z_\pi}{2\pi^2}\int_0^1 dx x(1-2x)\bar{\mathcal{C}}_1(\sigma_2) - \frac{N_c Z_\pi}{4\pi^2}\int_0^1 dx\frac{(1-x)\left(2m_\pi^2 - t\right)}{t}\bar{\mathcal{C}}_1(\sigma_1) + \frac{N_c Z_\pi}{4\pi^2}\int_0^1 dx\int_0^{1-x} dy\frac{\left(2m_\pi^2 - t\right)}{t}\bar{\mathcal{C}}_1(\sigma_7), \tag{38}$$

$$B_{2,0}(t) = \frac{N_c Z_\pi}{2\pi^2}\int_0^1 dx\int_0^{1-x} dy \times m_\pi M(1-x-y)\frac{1}{\sigma_7}\bar{\mathcal{C}}_2(\sigma_7), \tag{39}$$

$B_{2,2}(t)$ is zero in the NJL model. The dressed form factors are $F_\pi^D(Q^2) = F_\pi(Q^2)F_{1\rho}(Q^2)$, $B_{1,0}^D(Q^2) = B_{1,0}(Q^2)F_{1\rho}(Q^2)$, $A_{2,0}^D(Q^2) = A_{2,0}(Q^2)F_{1\rho}(Q^2)$, $A_{2,2}^D(Q^2) = A_{2,2}(Q^2)F_{1\rho}(Q^2)$, $B_{2,0}^D(Q^2) = B_{2,0}(Q^2)F_{1\rho}(Q^2)$. Values at $t = 0$ of the GFFs in the NJL model are given in Table 2.

The experimental data on electromagnetic form factor is well described by a monopole form

$$F_\pi^{mon}(Q^2) = \frac{1}{1 + Q^2/M^2}, \tag{40}$$

with a fit of the combined data from Refs. [45,46] giving $M = 0.719(5)$ GeV, which is plotted in Fig. 6, it is quite close to our dressed vector FF $F_\pi^D(Q^2)$.

In Refs. [47,48], the lattice data have been extrapolated to the physical pion mass through a simple quadratic (in m_π) expression, and then fitted by the following pole form

$$\frac{GFF_j^{lQCD}(Q^2)}{GFF_j^{lQCD}(0)} = \frac{1}{\left[1 + Q^2/(p_j M_j^2)\right]^{p_j}}, \tag{41}$$

where p_j and M_j are pairs of adjustable parameters, shown in Table 3.

In Fig. 6, the lattice data are represented by shaded areas, produced by the envelope of curves that fit the lattice data with their uncertainties. Comparison with the lattice QCD (lQCD) data is

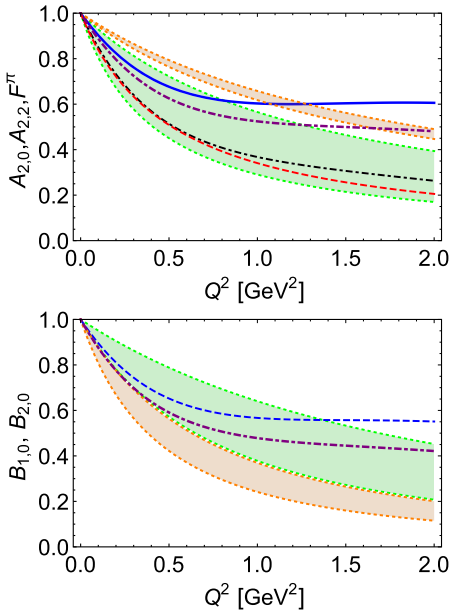

Fig. 6. *Upper panel* – Pion form factors computed from the vector GPD, normalized to their values at $Q^2 = 0$: dot-dashed purple curve – $A^D_{2,0}$; blue solid curve – $A^D_{2,2}$; dot-dashed black curve – F^D_π; dashed red curve – F^{mon}_π. For comparison, lQCD results in Eq. (41) use data in Table 3: dotted orange curve within like-colored band – $A^D_{2,0}$ and dotted green curve within like-colored band – $A^D_{2,2}$; *lower panel* – Pion form factors computed from the tensor GPD: dot-dashed purple curve – $B^D_{1,0}$; and dashed green curve – $B^D_{2,0}$. For comparison, lQCD results in Eq. (41) use data in Table 3: dotted orange curve within like-colored band – $B^D_{1,0}$ and dotted green curve within like-colored band – $B^D_{2,0}$. (For interpretation of the colors in the figure(s), the reader is referred to the web version of this article.)

Table 3
Lattice data of Eq. (41) from Refs. [47,48].

GFF	p_j	M_j
$A_{2,0}$	1	1.329 ± 0.058
$A_{2,2}$	1	0.890 ± 0.250
$B_{1,0}$	1.6	0.756 ± 0.095
$B_{2,0}$	1.6	1.130 ± 0.265

significant, but the lQCD form factors were computed using quite large m_π quantitative coincide cannot be expected so well. From the diagram we can see that F^D_π is very close to the monopole form F^{mon}_π extracted from experiment, especially in small Q^2 region. The dressed $A^D_{2,0}$ are not so well compared with lattice data, $A^D_{2,2}$ is well compared with lattice data in small Q^2 region, when Q^2 is larger, it is harder than lattice data. The dressed $B^D_{1,0}$ is harder than the lattice data. $B^D_{2,0}$ is better in small Q^2 region, when Q^2 is larger, it is harder than lattice data.

2.3.4. Impact parameter dependent PDFs

In order to define impact parameter dependent PDFs one first needs to localize pion in the transverse direction. The momentum state can be defined as

$$|p^+, \boldsymbol{R}_\perp = \boldsymbol{0}_\perp\rangle = \mathcal{N}\int \frac{d^2\boldsymbol{p}_\perp}{(2\pi)^2}|p^+, \boldsymbol{p}_\perp\rangle, \tag{42}$$

where $|p^+, \boldsymbol{p}_\perp\rangle$ are light-cone helicity eigenstates. $\mathcal{N}$ is a normalization factor, $\boldsymbol{R}_\perp$ is transverse center of momentum, which is defined as

$$\boldsymbol{R}_\perp = \frac{\sum_i x_i \boldsymbol{b}_{\perp,i}}{\sum_i x_i} = \sum_i x_i \boldsymbol{b}_{\perp,i}, \tag{43}$$

where we sum over all partons in the pion, $\boldsymbol{b}_\perp$ is the distance from the transverse center of the momentum.

The impact parameter dependent PDFs are defined as

$$\begin{aligned} q\left(x, \boldsymbol{b}_\perp^2\right) &\equiv \langle p^+, \boldsymbol{R}_\perp = \boldsymbol{0}_\perp|\hat{O}\left(x, \boldsymbol{b}_\perp\right)|p^+, \boldsymbol{R}_\perp = \boldsymbol{0}_\perp\rangle \\ &= \int \frac{dx^-}{4\pi} e^{ixp^+x^-}\langle p^+, \boldsymbol{0}_\perp|\bar{q}(-\frac{x^-}{2}, \boldsymbol{b}_\perp)\gamma^+ q(\frac{x^-}{2}, \boldsymbol{b}_\perp)|p^+, \boldsymbol{0}_\perp\rangle \\ &= |\mathcal{N}|^2 \int \frac{d^2\boldsymbol{p}_\perp}{(2\pi)^2}\int \frac{d^2\boldsymbol{p}'_\perp}{(2\pi)^2}\int \frac{dx^-}{4\pi} e^{ixp^+x^-} e^{i\boldsymbol{b}_\perp\cdot(\boldsymbol{p}_\perp - \boldsymbol{p}'_\perp)} \\ &\times \langle p^+, \boldsymbol{p}'_\perp|\bar{q}(-\frac{x^-}{2}, \boldsymbol{0}_\perp)\gamma^+ q(\frac{x^-}{2}, \boldsymbol{0}_\perp)|p^+, \boldsymbol{p}_\perp\rangle \\ &= \int \frac{d^2\boldsymbol{q}_\perp}{(2\pi)^2} e^{-i\boldsymbol{b}_\perp\cdot\boldsymbol{q}_\perp} H\left(x, 0, -\boldsymbol{q}_\perp^2\right), \end{aligned} \tag{44}$$

which means the impact parameter dependent PDFs are the Fourier transform of GPDs at $\xi = 0$.

When $\xi = 0$ and $t \neq 0$, GPDs become

$$H\left(x, 0, -\boldsymbol{q}_\perp^2\right) = \frac{N_c Z_\pi}{4\pi^2}\bar{\mathcal{C}}_1(\sigma_1) + \frac{N_c Z_\pi}{4\pi^2}\int_0^{1-x} d\alpha \left(2xm_\pi^2 + x\boldsymbol{q}_\perp^2 - \boldsymbol{q}_\perp^2\right)\frac{1}{\sigma_8}\bar{\mathcal{C}}_2(\sigma_8), \tag{45}$$

$$E\left(x, 0, -\boldsymbol{q}_\perp^2\right) = \frac{N_c Z_\pi}{2\pi^2}\int_0^{1-x} d\alpha m_\pi M\frac{1}{\sigma_8}\bar{\mathcal{C}}_2(\sigma_8), \tag{46}$$

where $x \in [0, 1]$. After the two-dimensional Fourier transform

$$\begin{aligned} u\left(x, \boldsymbol{b}_\perp^2\right) &= \frac{N_c Z_\pi}{4\pi^2}\int \frac{d^2\boldsymbol{q}_\perp}{(2\pi)^2} e^{-i\boldsymbol{b}_\perp\cdot\boldsymbol{q}_\perp}\bar{\mathcal{C}}_1(\sigma_1) + \frac{N_c Z_\pi}{32\pi^3}\int_0^{1-x} d\alpha \int d\tau \\ &\times \frac{(x-1)\left(4 - \frac{\boldsymbol{b}_\perp^2}{\alpha(1-\alpha-x)\tau}\right) + 8\alpha x(1-\alpha-x)\tau m_\pi^2}{4\alpha^2\tau^2(1-\alpha-x)^2} \\ &\times e^{-\tau\left(M^2 - x(1-x)m_\pi^2\right)} e^{-\frac{\boldsymbol{b}_\perp^2}{4\tau(1-\alpha-x)\alpha}}, \end{aligned} \tag{47}$$

$$u_T\left(x, \boldsymbol{b}_\perp^2\right) = \frac{N_c Z_\pi}{16\pi^3}\int_0^{1-x} d\alpha \int d\tau \frac{m_\pi M}{\alpha(1-\alpha-x)\tau} e^{-\frac{\boldsymbol{b}_\perp^2}{4\tau(1-\alpha-x)\alpha}} e^{-\tau\left(M^2 - x(1-x)m_\pi^2\right)}, \tag{48}$$

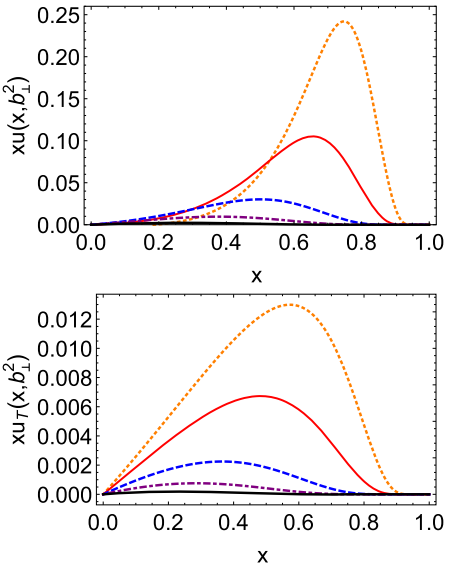

Fig. 7. Impact parameter space PDFs: upper panel – $xu\left(x, \boldsymbol{b}_\perp^2\right)$, the $\delta^2(\boldsymbol{b}_\perp)$ component first line of Eq. (47) – is suppressed in the image, and lower panel – $xu_T\left(x, \boldsymbol{b}_\perp^2\right)$ both panels with $\boldsymbol{b}_\perp^2 = 0.5$ GeV^{-2} — orange dotted curve, $\boldsymbol{b}_\perp^2 = 1$ GeV^{-2} — red solid curve, $\boldsymbol{b}_\perp^2 = 2.5$ GeV^{-2} — blue dashed curve, $\boldsymbol{b}_\perp^2 = 5$ GeV^{-2} — purple dot-dashed curve, $\boldsymbol{b}_\perp^2 = 10$ GeV^{-2} — thick black solid curve.

for $u\left(x, \boldsymbol{b}_\perp^2\right)$, when integrating $\boldsymbol{b}_\perp$ one can get PDF $u(x)$ in Eq. (27), the impact parameter dependent PDFs are plotted in Fig. 7.

$H(x, 0, -\boldsymbol{q}_\perp^2)$ should be independent of $-\boldsymbol{q}_\perp^2$ when $x \to 1$ as Refs. [19,48]. From Eq. (45) we can see that the first term is independent of $-\boldsymbol{q}_\perp^2$, for the second term, $\alpha \in [0, 1-x]$, when $x \to 1$, this term will vanish.

The width distribution of u quark in the pion for a given momentum fraction x is defined as [19]

$$\langle \boldsymbol{r}_\perp^2 \rangle_x = \frac{\int d^2\boldsymbol{b}_\perp \boldsymbol{b}_\perp^2 u(x, \boldsymbol{b}_\perp^2)}{\int d^2\boldsymbol{b}_\perp u(x, \boldsymbol{b}_\perp^2)}, \tag{49}$$

when $x \to 1$, this average impact parameter should be zero because the struck quark becomes closer to the center of momentum since its weight increases. The denominator of Eq. (49) is pion PDF $u(x)$. For the numerator from Eq. (47) we could see that the first term is a $\delta^2(\boldsymbol{b}_\perp)$ term, this term vanish. The second term is limited in the region $\alpha \in [0, 1-x]$, when $x \to 1$, this term will vanish, so our $\langle \boldsymbol{r}_\perp^2 \rangle_x$ satisfies the requirement. That's also can be seen from Fig. 8, when $x \to 1$, the value of $\langle \boldsymbol{r}_\perp^2 \rangle_x$ becomes zero. What's more, the figure shows that the width distribution $\langle \boldsymbol{r}_\perp^2 \rangle_x$ monotone decreasing with x as Ref. [48]. When $x = 0$, $\langle \boldsymbol{r}_\perp^2 \rangle_x^{1/2} = 0.649$ fm is the same magnitude as charge radius r_π.

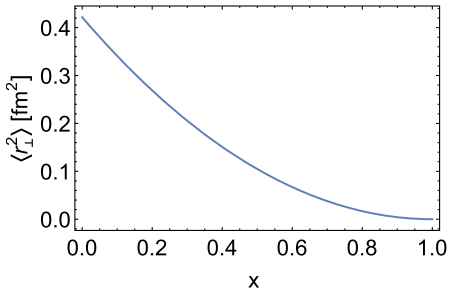

Fig. 8. The width of the distribution of u quark in the pion for a given momentum fraction x defined in Eq. (49).

3. Light-front wave functions

In principle, LFWFs can be obtained by solving the eigenvalue equation of the light-cone Hamiltonian using either analytical or numerical methods. LFWFs of hadrons can be labeled as $\psi_n^H(x_i, \boldsymbol{k}_{i\perp}, \lambda_i)$, x_i is the light-front momentum fractions of the n constituents, $\boldsymbol{k}_{i\perp}$ the transverse momentum components, and λ_i the parton helicities. For pion, the leading Fock state LFWF is the two quark state $\psi_2(x, \boldsymbol{k}_\perp, \lambda, \lambda')$.

3.1. The definition and calculation of pion LFWF

The most general pion Bethe-Salpeter vertex in the NJL model has the form

$$\Gamma_\pi(q) = \alpha_1\gamma_5 + \alpha_2 \not{q}\gamma_5, \tag{50}$$

and therefore the pion Bethe-Salpeter wave function is given by

$$\chi_\pi\left(k', k\right) = iS(k)\Gamma_\pi(q)iS(k-q), \tag{51}$$

$\varphi_\pi(x, \boldsymbol{k}_\perp)$ is given by

$$\varphi_\pi(x, \boldsymbol{k}_\perp) = \int \frac{dk^+dk^-}{2\pi}\delta(x - \frac{k^+}{q^+})\chi_\pi\left(k', k\right). \tag{52}$$

Pion LFWF in the NJL model is defined as [49,50]

$$\begin{aligned} &-2q^+\sqrt{x\bar{x}}\psi_2\left(x, \boldsymbol{k}_\perp, \lambda, \lambda'\right) \\ &= i\sqrt{6}\bar{u}\left(xq^+, \boldsymbol{k}_\perp, \lambda\right)\gamma^+\varphi_\pi(x, \boldsymbol{k}_\perp)\gamma^+ v\left(\bar{x}q^+, -\boldsymbol{k}_\perp, \lambda'\right), \end{aligned} \tag{53}$$

where $\bar{x} = 1 - x$, using the relationships in Ref. [49]

$$\bar{u}\left(xq^+, \boldsymbol{k}_\perp, \lambda\right)\gamma^+(\not{k} + M) = 2xq^+\bar{u}\left(xq^+, \boldsymbol{k}_\perp, \lambda\right), \tag{54}$$

$$(\not{k} - \not{q} + M)\gamma^+ v\left(\bar{x}q^+, -\boldsymbol{k}_\perp, \lambda'\right) = -2\bar{x}q^+ v\left(\bar{x}q^+, -\boldsymbol{k}_\perp, \lambda'\right), \tag{55}$$

we arrive at

$$\begin{aligned} \psi_2\left(x, \boldsymbol{k}_\perp, \lambda, \lambda'\right) = i\sqrt{6}\int \frac{dk^+dk^-}{\pi}\delta\left(x - \frac{k^+}{q^+}\right)\frac{\sqrt{x(1-x)}}{\left(k^2 - M^2\right)\left((k-q)^2 - M^2\right)} \\ \times \bar{u}\left(xq^+, \boldsymbol{k}_\perp, \lambda\right)\gamma^+(\alpha_1\gamma_5 + \alpha_2\not{q}\gamma_5)\gamma^+ v\left(\bar{x}q^+, -\boldsymbol{k}_\perp, \lambda'\right), \end{aligned} \tag{56}$$

in the NJL model, $\alpha_1 = \sqrt{Z_\pi}$, we do not consider the mixing of the pseudoscalar and the pseudovector interaction terms in the Bethe-Salpeter equation of pion, so $\alpha_2 = 0$, one arrives at the final form

$$\begin{aligned}\psi_2\left(x, \boldsymbol{k}_\perp, \lambda, \lambda'\right) &= \begin{pmatrix} \psi_{2\uparrow\uparrow} & \psi_{2\uparrow\downarrow} \\ \psi_{2\downarrow\uparrow} & \psi_{2\downarrow\downarrow} \end{pmatrix} \\ &= \frac{\sqrt{6}\sqrt{Z_\pi}}{\boldsymbol{k}_\perp^2 + M^2 + m_\pi^2(x-1)x} \begin{pmatrix} -k_{-\lambda} & M \\ -M & -k_{-\lambda'} \end{pmatrix}, \end{aligned} \tag{57}$$

where λ is the parton helicity, $k_\lambda \equiv k_1 + i\lambda k_2$, $\lambda = 1$, $\lambda' = -1$, $\psi_{2\uparrow\uparrow}$ and $\psi_{2\downarrow\downarrow}$ are spin parallel $S_z = \pm 1$, $\psi_{2\uparrow\downarrow}$ and $\psi_{2\downarrow\uparrow}$ are spin anti-parallel $S_z = 0$. It has been pointed out by Leutwyler that both spin alignments should contribute to the pion LFWFs [51,52].

3.2. The properties of pion LFWF

3.2.1. Normalization

The normalization condition is

$$\sum_{\lambda,\lambda'} \int_0^1 dx \int \frac{d^2\boldsymbol{k}_\perp}{16\pi^3} |\, \psi_2\left(x, \boldsymbol{k}_\perp, \lambda, \lambda'\right) |^2 = 1. \tag{58}$$

It is of course a critical assumption that the probability to find pion in its valence state is one. In this way we enforce a constituent picture by fiat, and it is clear that such an assumption has to be checked explicitly by comparing with phenomenology.

$$1 = \frac{3Z_\pi}{4\pi^2} \int_0^1 dx \bar{\mathcal{C}}_1(\sigma_1) + \frac{3Z_\pi}{2\pi^2} \int_0^1 dx x(1-x) m_\pi^2 \frac{1}{\sigma_1} \bar{\mathcal{C}}_2(\sigma_1), \tag{59}$$

this is the same as Eq. (28), so our results satisfy the normalization condition.

3.2.2. Pion decay constant

Pion decay constant appears in the semi-leptonic process $\pi \to \mu\nu$ is the second restrict on the LFWF, generating the following constraint,

$$\int_0^1 dx \int \frac{d^2\boldsymbol{k}_\perp}{16\pi^3} \psi_{2\uparrow\downarrow}(x, \boldsymbol{k}_\perp) = \frac{f_\pi}{2\sqrt{6}}, \tag{60}$$

in Section 2, we use $f_\pi = 0.092$ GeV to define the parameters. Now we get the decay constant from LFWF,

$$f_\pi = 0.092 \quad \text{GeV}, \tag{61}$$

it is exactly the same.

3.2.3. Constraint from $\pi^0 \to 2\gamma$

This constraint was derived by Brodsky and Lepage within an analysis of the $\pi\gamma$ transition form factor, Eq. (2.23) in Ref. [20], assumes very simple form,

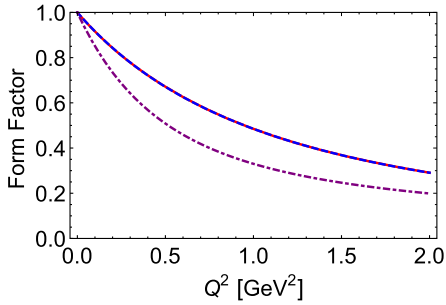

Fig. 9. The pion FF calculated from two different methods, bare vector FF $F_\pi(Q^2)$ from vector GPD in Eq. (33a) – red solid curve; the dressed FF $F_\pi^D(Q^2)$ – dot-dashed purple curve; the bare FF $F_\pi(Q^2)$ from LFWF in Eq. (65) – dashed green curve.

$$\int_0^1 dx \psi_{2\uparrow\downarrow}(x, \mathbf{0}_\perp) = \frac{\sqrt{6}}{f_\pi}, \tag{62}$$

inserting into the LFWF in Eq. (57),

$$f_\pi = 0.093 \quad \text{GeV}, \tag{63}$$

this can also be check of our results.

3.2.4. Pion form factor

We proceed by calculating the pion electromagnetic form factor

$$F_\pi\left(Q^2\right) = \sum_{\lambda,\lambda'} \int_0^1 dx \int \frac{d^2\boldsymbol{k}_\perp}{16\pi^3} \psi_2^\dagger\left(x, \boldsymbol{k}'_\perp, \lambda, \lambda'\right) \psi_2\left(x, \boldsymbol{k}_\perp, \lambda, \lambda'\right), \tag{64}$$

the transverse momentum of the struck quark $\boldsymbol{k}'_\perp = \boldsymbol{k}_\perp + (1-x)\boldsymbol{q}_\perp$.

$$\begin{aligned} F_\pi\left(Q^2\right) = & \frac{3Z_\pi}{4\pi^2} \int_0^1 dx \bar{\mathcal{C}}_1(\sigma_1) \\ & - \frac{3Z_\pi}{4\pi^2} \int_0^1 dx \int_0^1 dy (2m_\pi^2 x(x-1) + (1-x)^2 Q^2) \frac{1}{\sigma_9} \bar{\mathcal{C}}_2(\sigma_9), \end{aligned} \tag{65}$$

which is plotted in Fig. 9, it can be seen that $F_\pi(Q^2)$ is coincide with $F_\pi(Q^2)$ in Eq. (34).

When $Q^2 = 0$, we should get the normalization condition

$$F_\pi(0) = \frac{3Z_\pi}{4\pi^2} \int_0^1 dx \bar{\mathcal{C}}_1(\sigma_1) + \frac{3Z_\pi}{2\pi^2} \int_0^1 dx x(1-x) m_\pi^2 \frac{1}{\sigma_1} \bar{\mathcal{C}}_2(\sigma_1), \tag{66}$$

it is exactly the same as the normalization condition in Eq. (59). The pion root mean square radius r_π is determined by the slope of FF at zero momentum transfer,

$$F_\pi\left(Q^2\right) \equiv 1 - \frac{r_\pi^2}{6} Q^2 + O\left(Q^4\right), \tag{67}$$

then

$$\langle r_\pi^2 \rangle = -6 \frac{\partial F_\pi\left(Q^2\right)}{\partial Q^2}|_{Q^2=0}, \tag{68}$$

we get $r_\pi = 0.46$ fm, with the dressed quark-photon vertex, $r_\pi^D = 0.63$ fm, it is much closer to the experiment data 0.66 fm.

3.2.5. Transverse size

The r.m.s. transverse momentum is defined as [50]

$$\begin{aligned}\left\langle \boldsymbol{k}_\perp^2 \right\rangle &\equiv \sum_{\lambda,\lambda'} \int_0^1 dx \int \frac{d^2\boldsymbol{k}_\perp}{16\pi^3} \boldsymbol{k}_\perp^2 |\psi_2\left(x, \boldsymbol{k}_\perp, \lambda, \lambda'\right)|^2 \\ &= \frac{3Z_\pi}{4\pi^2} \int_0^1 dx \mathcal{C}_0(\sigma_1) + \frac{3Z_\pi}{4\pi^2} \int_0^1 dx x(1-x) m_\pi^2 \bar{\mathcal{C}}_1(\sigma_1) \\ &= (0.481 \quad \text{GeV})^2. \end{aligned} \tag{69}$$

In order to confirm that pion is highly relativistic, we should have $\left\langle \boldsymbol{k}_\perp^2 \right\rangle^{1/2} \simeq M > m_\pi$. This transverse momentum, compare with the result $\left\langle \boldsymbol{k}_\perp^2 \right\rangle^{1/2} = 0.21$ GeV from an interaction with QCD-like momentum dependence model [53], is larger. That's because NJL model is contact interaction, thus produce a hard $\left\langle \boldsymbol{k}_\perp^2 \right\rangle$ distribution. Translated r.m.s. transverse momentum into a transverse size scale $R_\perp$.

$$R_\perp^2 \equiv \frac{1}{\left\langle \boldsymbol{k}_\perp^2 \right\rangle} = (0.410 \quad \text{fm})^2. \tag{70}$$

It is slightly smaller than the bare charge radius r_π. The dimensionless quantity $C = f_\pi R_\perp$ [54] connect "core radius" $R_\perp$ with the decay constant f_π is 0.191, which is in accordance with the result $C \simeq 0.2$ in Ref. [55].

3.2.6. Parton distribution function

The valence structure function of pion is given by integrating the squares of LFWF

$$\begin{aligned} u(x) &= \sum_{\lambda,\lambda'} \int \frac{d^2\boldsymbol{k}_\perp}{16\pi^3} |\psi_2\left(x, \boldsymbol{k}_\perp, \lambda, \lambda'\right)|^2 \\ &= \frac{3Z_\pi}{4\pi^2} \bar{\mathcal{C}}_1(\sigma_1) + \frac{3Z_\pi}{2\pi^2} x(1-x) m_\pi^2 \frac{1}{\sigma_1} \bar{\mathcal{C}}_2(\sigma_1), \end{aligned} \tag{71}$$

it is the same as PDF in Eq. (27) from pion vector GPD, so it satisfies the consistency in Eq. (28). We find that the average value of the momentum fraction x carried by u quark

$$\langle x \rangle = \int_0^1 x u(x) dx = \frac{1}{2}, \tag{72}$$

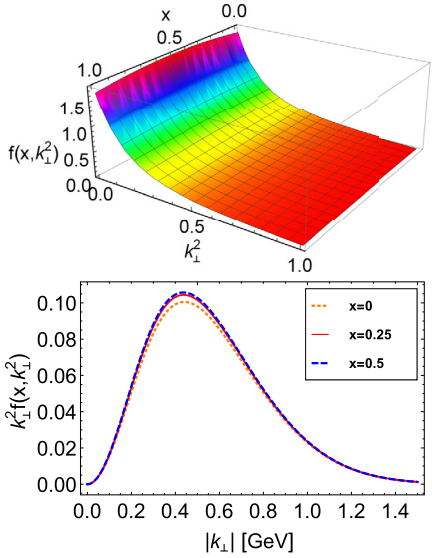

Fig. 10. *Upper panel* – pion TMD, around the line $x = 1/2$ it is symmetric; and *lower panel* – $k_\perp^2 f\left(x, k_\perp^2\right)$, $x = 0$ – the red dotted curve, $x = 0.25$ – the red curve, $x = 0.5$ – the green dashed curve.

it means that the quarks share the same amount of longitudinal momentum averagely.

3.2.7. Parton distribution amplitude

PDA was introduced to depict hard exclusive processes, which can be obtained

$$\phi(x) = \frac{2\sqrt{6}}{f_\pi} \int \frac{d^2\boldsymbol{k}_\perp}{16\pi^3} \psi_{2\uparrow\downarrow}(x, \boldsymbol{k}_\perp) = \frac{3M\sqrt{Z_\pi}}{4\pi^2 f_\pi} \bar{\mathcal{C}}_1(\sigma_1), \tag{73}$$

PDA satisfy the relationship $\int_0^1 \phi(x)dx = 1$.

3.2.8. Transverse momentum dependent parton distribution

The unpolarized TMD is given by

$$\begin{aligned} f\left(x, \boldsymbol{k}_\perp^2\right) &= \sum_{\lambda,\lambda'} \frac{1}{16\pi^3} \left|\psi_2\left(x, \boldsymbol{k}_\perp, \lambda, \lambda'\right)\right|^2 \\ &= \frac{3Z_\pi}{2\pi^3} \frac{1}{\sigma_{12}} \bar{\mathcal{C}}_2(\sigma_{12}) + \frac{3Z_\pi}{4\pi^3} x(1-x) m_\pi^2 6 \frac{1}{\sigma_{12}^2} \bar{\mathcal{C}}_3(\sigma_{12}), \end{aligned} \tag{74}$$

this TMD describing the valence quark in the pion, we plot it in Fig. 10, it is symmetric around the line $x = 1/2$. One can get pion PDF $u(x)$ when integrating $\boldsymbol{k}_\perp$ of TMD. For comparison, we note that Ref. [43] also computed TMD in the NJL model use Pauli-Villars procedure. They obtained results that agree semi-quantitatively with our TMD, this is because NJL model results are sensitive to the regularization scheme employed.

3.2.9. Generalized parton distribution

According to Ref. [56], the relationship between LFWF and GPD in the region $\xi \leq x \leq 1$ reads,

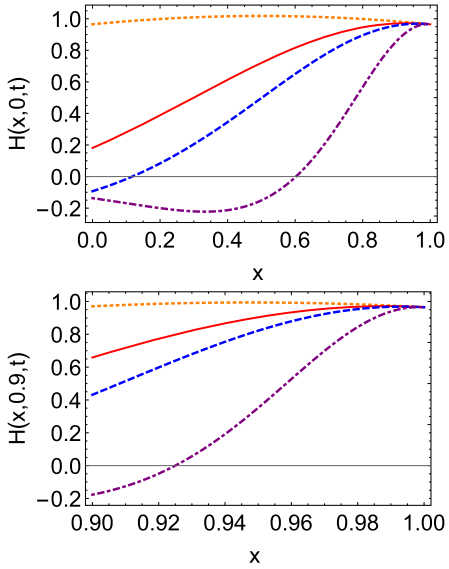

Fig. 11. The LFWF GPD: upper panel – $\xi = 0$ in the region $x \in [0, 1]$, and lower panel – $\xi = 0.9$ in the region $x \in [0.9, 1]$, both panels with $t = 0$ GeV^2 — orange dotted curve, $t = -0.5$ GeV^2 — red solid curve, $t = -1$ GeV^2 — blue dashed curve, $t = -5$ GeV^2 — purple dot-dashed curve.

$$H(x,\xi,t) = \sum_{\lambda'\lambda} \int \frac{d^2\boldsymbol{k}_\perp}{16\pi^3} \psi_2^\dagger\left(x'', \boldsymbol{k}''_\perp, \lambda'\right) \psi_2\left(x', \boldsymbol{k}'_\perp, \lambda\right), \tag{75}$$

where

$$x'' = \frac{x-\xi}{1-\xi}, \qquad \boldsymbol{k}''_\perp = \boldsymbol{k}_\perp + \frac{1-x}{1-\xi}\frac{\boldsymbol{q}_\perp}{2}, \tag{76a}$$

$$x' = \frac{x+\xi}{1+\xi}, \qquad \boldsymbol{k}'_\perp = \boldsymbol{k}_\perp - \frac{1-x}{1+\xi}\frac{\boldsymbol{q}_\perp}{2}, \tag{76b}$$

then we can get

$$\begin{aligned} H(x,\xi,t) = {} & \frac{3Z_\pi}{8\pi^2}\theta_{\xi 1}\bar{\mathcal{C}}_1(\sigma_3) + \frac{3Z_\pi}{8\pi^2}\theta_{\xi 1}\bar{\mathcal{C}}_1(\sigma_4) + \frac{3Z_\pi}{4\pi^2}\int_0^1 dz\theta_{\xi 1}(1-x)\frac{1}{\sigma_{11}}\bar{\mathcal{C}}_2(\sigma_{11}) \\ & \times\left(\frac{(x-\xi)}{(1-\xi)^2}m_\pi^2 + \frac{(x+\xi)}{(1+\xi)^2}m_\pi^2 + \frac{(1-x)t}{(1-\xi)^2(1+\xi)^2}\right), \end{aligned} \tag{77}$$

which is plotted in Fig. 11. From the diagrams we could see that GPD is monotonic increasing with t in the region $x \in [\xi, 1]$, so with fixed x and ξ, GPD has a maximum value at $t = 0$. In the forward limit, GPD reduces to PDF $u(x)$. When $\xi = 0$, $x \in [0, 1]$, integrating over x, one can get FF in Eq. (65).

3.2.10. Positivity bound of LFWF GPD

According to Refs. [57,58], using the Schwartz inequality and the momentum representation of pion LFWFs. GPD should satisfy the relationship

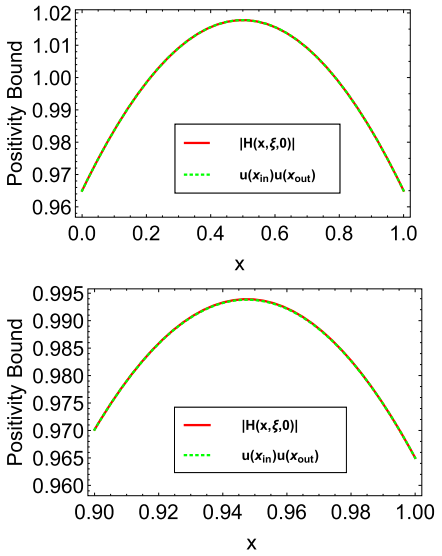

Fig. 12. The positive bound for $t = 0$, $\xi = 0, 0.9$ in the region $\xi \leq x \leq 1$.

$$|H(x,\xi,t)| \leq \sqrt{u(x_{in})u(x_{out})}, \quad \xi \leq x \leq 1, \tag{78}$$

where $x_{in} = \frac{x+\xi}{1+\xi}$, $x_{out} = \frac{x-\xi}{1-\xi}$.

For our results, in the chiral limit (when $t = 0$)

$$H(x,\xi,0) = \frac{N_c Z_\pi}{4\pi^2}\int d\tau \frac{1}{\tau} e^{-\tau M^2}, \tag{79}$$

$$\sqrt{u(x_{in})u(x_{out})} = \frac{N_c Z_\pi}{4\pi^2}\int d\tau \frac{1}{\tau} e^{-\tau M^2}, \tag{80}$$

the two terms are equal. From Fig. 11, we can see that in the region $\xi \leq x \leq 1$, with different t, $t = 0$ is the largest, so in the $t = 0$ case, if Eq. (78) is true, GPD with other values of t will also satisfy the relationship. So in Fig. 12, we have plot the diagrams of $\sqrt{u(x_{in})u(x_{out})}$, $H(x,\xi,0)$ from the LFWF in the region $\xi \leq x \leq 1$ with different ξ. From the diagrams we could see, $H(x,\xi,0)$ and $\sqrt{u(x_{in})u(x_{out})}$ are coincided at $\xi = 0$ and $\xi = 0.9$, which means our GPD satisfies the positivity bound.

3.2.11. Impact parameter dependent PDF

In the case $\xi = 0$,

$$\begin{aligned} H(x,0,-\boldsymbol{q}_\perp^2) = {} & \frac{3Z_\pi}{4\pi^2}\bar{\mathcal{C}}_1(\sigma_1) \\ & - \frac{3Z_\pi}{4\pi^2}\int_0^1 dz \left(2x(x-1)m_\pi^2 + (1-x)^2\boldsymbol{q}_\perp^2\right)\frac{1}{\sigma_{10}}\bar{\mathcal{C}}_2(\sigma_{10}), \end{aligned} \tag{81}$$

when taking a two-dimensional Fourier transform of $\boldsymbol{q}_\perp$, one arrives at

$$u(x,\boldsymbol{b}_\perp^2) = \int \frac{d^2\boldsymbol{q}_\perp}{(2\pi)^2}\int d\tau e^{-i\boldsymbol{b}_\perp\cdot\boldsymbol{q}_\perp} H(x,0,-\boldsymbol{q}_\perp^2)$$

$$= \frac{3Z_\pi}{4\pi^2}\int \frac{d^2\boldsymbol{q}_\perp}{(2\pi)^2} e^{-i\boldsymbol{b}_\perp\cdot\boldsymbol{q}_\perp}\bar{\mathcal{C}}_1(\sigma_1)$$
$$- \frac{3Z_\pi}{4\pi^2}\int_0^1 dz \int \frac{d^2\boldsymbol{q}_\perp}{(2\pi)^2} e^{-i\boldsymbol{b}_\perp\cdot\boldsymbol{q}_\perp}$$
$$\times \left(2x(x-1)m_\pi^2 + (1-x)^2\boldsymbol{q}_\perp^2\right)\frac{1}{\sigma_{10}}\bar{\mathcal{C}}_2(\sigma_{10}), \tag{82}$$

it is the same as impact parameter dependent PDF in Eq. (47).

4. Summary and outlook

In this paper, we calculated pion generalized parton distributions (GPDs) and light-front wave functions (LFWFs) in the Nambu–Jona-Lasinio (NJL) model, use the proper time regularization scheme with a infrared cutoff to mimic confinement.

The results of pion vector and tensor GPDs satisfy their basic properties very well. In the forward limit vector GPD reduces to pion parton distribution function (PDF), by integrating x one can get pion form factors (FFs), GPDs also satisfy the polynomiality condition and symmetry properties. Besides, we discussed the generalized FFs (GFFs) θ_1 and θ_2, which relate to the quark pressure distribution and quark mass distribution respectively. The pion radius from the bare quark-photon vertex is too small, so we considered dressed quark-photon vertex from the inhomogeneous Bethe-Salpeter equation. The dressed pion electromagnetic FF is very close to the monopole form F_π^{mon} extracted from experimental data, especially in small Q^2 region. The dressed quark mass distribution and the dressed quark pressure distribution are harder than electromagnetic FF and the lattice data. The tensor anomalous magnetic moment $B^D_{1,0}$ and the generalized tensor form factor $B^D_{2,0}$ are harder than lattice data, $B^D_{1,0}$ is generally softer than $B^D_{2,0}$. The calculation of the leading Fock state pion LFWF is accomplished in the second section. PDF, parton distribution amplitude (PDA), FF, GPD that can be computed directly from the LFWF, satisfy the desired properties, observables f_π, r_π are the same as GPD results. More important, through comparison of pion PDF, impact parameter dependent PDF, FFs given by the vector GPD and LFWF, we find that they are exactly the same. This means the two methods give us the same picture of pion structure in the NJL model.

In summary, NJL model turns out to be rather good in describing the pion phenomenology, particularly considering that NJL model involves fairly simple calculations. NJL model also shows similar tendency with lattice data, this is an interesting phenomenon between the calculations performed in the two spaces, this can give us a special attention to the problem of the analytic behavior.

In the future, on one hand, improving the present model, on the other hand, we would like to check whether this case will occur in other hadrons, for example, the simplest case, kaon. Similar analyses for kaon would reveal physical effects that arise from constructive interference between Nature's two mass generating mechanisms: EHM and Higgsboson mechanism.

CRediT authorship contribution statement

Jin-Li Zhang, Meng-Yun Lai, Hong-Shi Zong and Jia-Lun Ping were responsible for the conceptualization. Jin-Li Zhang carried out the calculations. All authors contributed to the writing.

Declaration of competing interest

The authors declare that they have no known competing financial interests or personal relationships that could have appeared to influence the work reported in this paper.

Acknowledgements

We are grateful for constructive comments and technical assistance from Zhu-Fang Cui. Work supported by: National Natural Science Foundation of China (under grant nos. 11805097, 11775118, 11535005, 12075117, 11690030), and Jiangsu Provincial Natural Science Foundation of China (under grant no. BK20180323).

Appendix A. Useful formulae

Here we use the gamma-functions ($n \in \mathbb{Z}, n \geq 0$)

$$\mathcal{C}_0(z) := \int_0^\infty \frac{s}{s+z} ds = \int_{\tau_{uv}^2}^{\tau_{ir}^2} d\tau \frac{1}{\tau^2} e^{-\tau z}, \tag{A.1a}$$

$$\mathcal{C}_n(z) := (-)^n \frac{\sigma^n}{n!} \frac{d^n}{d\sigma^n} \mathcal{C}_0(\sigma), \tag{A.1b}$$

$$\bar{\mathcal{C}}_i(z) := \frac{1}{z} \mathcal{C}_i(z). \tag{A.1c}$$

The bubble diagrams have the form

$$\Pi_{PP}(q^2)\delta_{ij} = 3i \int \frac{d^4k}{(2\pi)^4} \mathrm{Tr}[\gamma^5 \tau_i S(k) \gamma^5 \tau_j S(k+q)], \tag{A.2}$$

$$\Pi_{VV}(q^2)(g^{\mu\nu} - \frac{q^\mu q^\nu}{q^2})\delta_{ij} = 3i \int \frac{d^4k}{(2\pi)^4} \mathrm{Tr}[\gamma^\mu \tau_i S(k) \gamma^\nu \tau_j S(k+q)], \tag{A.3}$$

where the traces are over Dirac and isospin indices. Meson masses are then defined by the pole in the corresponding two body t matrix. The normalization factor is given by

$$Z_\pi^{-1} = -\frac{\partial}{\partial q^2} \Pi_{PP}(q^2)|_{q^2=m_\pi^2}, \tag{A.4}$$

this residue is interpreted as the effective meson-quark-quark coupling constant.

The σ functions are defined as

$$\sigma_1 = M^2 - x(1-x)m_\pi^2, \tag{A.5a}$$

$$\sigma_2 = M^2 - x(1-x)t = M^2 + x(1-x)Q^2, \tag{A.5b}$$

$$\sigma_3 = M^2 - \frac{x+\xi}{1+\xi}\frac{1-x}{1+\xi} m_\pi^2, \tag{A.5c}$$

$$\sigma_4 = M^2 - \frac{x-\xi}{1-\xi}\frac{1-x}{1-\xi} m_\pi^2, \tag{A.5d}$$

$$\sigma_5 = M^2 - \frac{1}{4}(1+\frac{x}{\xi})(1-\frac{x}{\xi})t, \tag{A.5e}$$

$$\sigma_6 = M^2 - \alpha\,(1-\alpha)\,m_\pi^2 - \left(\frac{\xi+x}{2\xi} - \alpha\frac{1+\xi}{2\xi}\right)\left(\frac{\xi-x}{2\xi} + \alpha\frac{1-\xi}{2\xi}\right)t\,, \tag{A.5f}$$

$$\sigma_7 = (x+y)(x+y-1)m_\pi^2 - xyt + M^2\,, \tag{A.5g}$$

$$\sigma_8 = M^2 + (1-\alpha-x)\alpha\boldsymbol{q}_\perp^2 - x\,(1-x)\,m_\pi^2\,, \tag{A.5h}$$

$$\sigma_9 = M^2 + m_\pi^2(x-1)x + (1-x)^2(1-y)yQ^2\,, \tag{A.5i}$$

$$\sigma_{10} = z(1-z)(1-x)^2\boldsymbol{q}_\perp^2 + x(x-1)m_\pi^2 + M^2\,, \tag{A.5j}$$

$$\sigma_{11} = -\frac{z(1-z)(1-x)^2t}{(\xi+1)^2(1-\xi)^2} + z\frac{(x-1)(x-\xi)}{(1-\xi)^2}m_\pi^2 + (1-z)\frac{(x-1)(\xi+x)}{(\xi+1)^2}m_\pi^2 + M^2\,, \tag{A.5k}$$

$$\sigma_{12} = \boldsymbol{k}_\perp^2 + x(x-1)m_\pi^2 + M^2 \tag{A.5l}$$

References

[1] L. Theussl, S. Noguera, V. Vento, Eur. Phys. J. A 20 (2004) 483, arXiv:nucl-th/0211036 [nucl-th].
[2] D. Muller, D. Robaschik, B. Geyer, F.M. Dittes, J. Horejsi, Fortschr. Phys. 42 (101) (1994), arXiv:hep-ph/9812448 [hep-ph].
[3] X.-D. Ji, Phys. Rev. D 55 (1997) 7114, arXiv:hep-ph/9609381 [hep-ph].
[4] A.V. Radyushkin, Phys. Rev. D 56 (1997) 5524, arXiv:hep-ph/9704207 [hep-ph].
[5] X.-D. Ji, J. Phys. G 24 (1998) 1181, arXiv:hep-ph/9807358 [hep-ph].
[6] M. Diehl, Phys. Rep. 388 (2003) 41, arXiv:hep-ph/0307382 [hep-ph].
[7] J.-L. Zhang, Z.-F. Cui, J. Ping, C.D. Roberts, Eur. Phys. J. C 81 (2021) 6, arXiv:2009.11384 [hep-ph].
[8] J.-L. Zhang, K. Raya, L. Chang, Z.-F. Cui, J. Morgado, C. Roberts, J. Rodríguez-Quintero, Phys. Lett. B 136158 (2021), arXiv:2101.12286 [hep-ph].
[9] K. Wijesooriya, P.E. Reimer, R.J. Holt, Phys. Rev. C 72 (065203) (2005), arXiv:nucl-ex/0509012 [nucl-ex].
[10] R.J. Holt, C.D. Roberts, Rev. Mod. Phys. 82 (2010) 2991, arXiv:1002.4666 [nucl-th].
[11] T. Nguyen, A. Bashir, C.D. Roberts, P.C. Tandy, Phys. Rev. C 83 (2011) 062201, arXiv:1102.2448 [nucl-th].
[12] P.C. Barry, N. Sato, W. Melnitchouk, C.-R. Ji, Phys. Rev. Lett. 121 (2018) 152001, arXiv:1804.01965 [hep-ph].
[13] I.C. Cloët, W. Bentz, A.W. Thomas, Phys. Rev. C 90 (2014) 045202, arXiv:1405.5542 [nucl-th].
[14] Z.-F. Cui, C. Chen, D. Binosi, F. de Soto, C.D. Roberts, J. Rodríguez-Quintero, S.M. Schmidt, J. Segovia, Phys. Rev. D 102 (2020) 014043, arXiv:2003.11655 [hep-ph].
[15] B.C. Tiburzi, G.A. Miller, Phys. Rev. D 67 (2003) 113004, arXiv:hep-ph/0212238 [hep-ph].
[16] X. Ji, Annu. Rev. Nucl. Part. Sci. 54 (2004) 413.
[17] A.V. Belitsky, X.-d. Ji, F. Yuan, Phys. Rev. D 69 (2004) 074014, arXiv:hep-ph/0307383 [hep-ph].
[18] M. Diehl, Eur. Phys. J. C 25 (2002) 223;
M. Diehl, Erratum, Eur. Phys. J. C 31 (2003) 277, arXiv:hep-ph/0205208 [hep-ph].
[19] M. Burkardt, Int. J. Mod. Phys. A 18 (2003) 173, arXiv:hep-ph/0207047 [hep-ph].
[20] G. Lepage, S.J. Brodsky, T. Huang, P. Mackenzie, Banff summer institute in particles and fields: QCD, in: Gauge Theories and Grand Unification Schemes, 1982, pp. 83–141.
[21] S.J. Brodsky, J.R. Hiller, D.S. Hwang, V.A. Karmanov, Phys. Rev. D 69 (2004) 076001, arXiv:hep-ph/0311218 [hep-ph].
[22] A.V. Radyushkin, Phys. Rev. D 58 (1998) 114008, arXiv:hep-ph/9803316 [hep-ph].
[23] M. Diehl, T. Feldmann, R. Jakob, P. Kroll, Eur. Phys. J. C 8 (409) (1999), arXiv:hep-ph/9811253 [hep-ph].
[24] A. Mukherjee, I.V. Musatov, H.C. Pauli, A.V. Radyushkin, Phys. Rev. D 67 (2003) 073014, arXiv:hep-ph/0205315 [hep-ph].
[25] A.V. Radyushkin, Phys. Rev. D 95 (2017) 056020, arXiv:1701.02688 [hep-ph].
[26] S.P. Klevansky, Rev. Mod. Phys. 64 (1992) 649.
[27] M. Buballa, Phys. Rep. 407 (205) (2005), arXiv:hep-ph/0402234 [hep-ph].
[28] J.-L. Zhang, C.-M. Li, H.-S. Zong, Chin. Phys. C 42 (2018) 123105.
[29] J.-L. Zhang, Y.-M. Shi, S.-S. Xu, H.-S. Zong, Mod. Phys. Lett. A 31 (2016) 1650086.
[30] Z.-F. Cui, J.-L. Zhang, H.-S. Zong, Sci. Rep. 7 (2017) 45937.

[31] Z.-F. Cui, I.C. Cloët, Y. Lu, C.D. Roberts, S.M. Schmidt, S.-S. Xu, H.-S. Zong, Phys. Rev. D 94 (2016) 071503, arXiv:1604.08454 [nucl-th].
[32] T. Hatsuda, T. Kunihiro, Phys. Rep. 247 (1994) 221, arXiv:hep-ph/9401310 [hep-ph].
[33] N. Ishii, W. Bentz, K. Yazaki, Phys. Lett. B 318 (1993) 26.
[34] N. Ishii, W. Bentz, K. Yazaki, Nucl. Phys. A 587 (1995) 617.
[35] I.C. Cloët, W. Bentz, A.W. Thomas, Phys. Lett. B 659 (2008) 214, arXiv:0708.3246 [hep-ph].
[36] Z.-F. Cui, J.-L. Zhang, D. Binosi, F. de Soto, C. Mezrag, J. Papavassiliou, C.D. Roberts, J. Rodríguez-Quintero, J. Segovia, S. Zafeiropoulos, Chin. Phys. C 44 (2020) 083102, arXiv:1912.08232 [hep-ph].
[37] N. Ishii, W. Bentz, K. Yazaki, Phys. Lett. B 301 (1993) 165.
[38] T. Ito, W. Bentz, I.C. Cloët, A.W. Thomas, K. Yazaki, Phys. Rev. D 80 (2009) 074008, arXiv:0906.5362 [nucl-th].
[39] H.H. Matevosyan, A.W. Thomas, W. Bentz, Phys. Rev. D 83 (2011) 074003, arXiv:1011.1052 [hep-ph].
[40] H.H. Matevosyan, A.W. Thomas, W. Bentz, Phys. Rev. D 86 (2012) 034025, arXiv:1205.5813 [hep-ph].
[41] G. Hellstern, R. Alkofer, H. Reinhardt, Nucl. Phys. A 625 (697) (1997), arXiv:hep-ph/9706551 [hep-ph].
[42] W. Bentz, A.W. Thomas, Nucl. Phys. A 696 (2001) 138, arXiv:nucl-th/0105022 [nucl-th].
[43] S. Noguera, S. Scopetta, J. High Energy Phys. 11 (2015) 102, arXiv:1508.01061 [hep-ph].
[44] P. Hagler, Phys. Rep. 490 (2010) 49, arXiv:0912.5483 [hep-lat].
[45] V. Tadevosyan, et al., Jefferson Lab F(pi), Phys. Rev. C 75 (2007) 055205, arXiv:nucl-ex/0607007.
[46] T. Horn, et al., Jefferson Lab F(pi)-2, Phys. Rev. Lett. 97 (192001) (2006), arXiv:nucl-ex/0607005.
[47] D. Brömmel, et al., UKQCD, QCDSF, Phys. Rev. Lett. 101 (2008) 122001, arXiv:0708.2249 [hep-lat].
[48] D. Brömmel, Pion Structure from the Lattice, Ph.D. thesis, Regensburg U, 2007.
[49] H.H. Liu, D.E. Soper, Phys. Rev. D 48 (1993) 1841.
[50] T. Heinzl, Methods of quantization, in: Proceedings, 39, Internationale Universitatswochen fur Kern- und Teilchenphysik, IUKT 39, Schladming, Austria, February 26-March 4, 2000, in: Lect. Notes Phys., vol. 572, 2001, p. 55, arXiv:hep-th/0008096 [hep-th].
[51] H. Leutwyler, Phys. Lett. B 48 (1974) 45.
[52] H. Leutwyler, Nucl. Phys. B 76 (1974) 413.
[53] S.-S. Xu, L. Chang, C.D. Roberts, H.-S. Zong, Phys. Rev. D 97 (2018) 094014, arXiv:1802.09552 [nucl-th].
[54] W. Weise, Int. Rev. Nucl. Phys. 1 (1984) 57.
[55] V. Bernard, R. Brockmann, W. Weise, Nucl. Phys. A 440 (1985) 605.
[56] S.J. Brodsky, M. Diehl, D.S. Hwang, Nucl. Phys. B 596 (2001) 99, arXiv:hep-ph/0009254 [hep-ph].
[57] P.V. Pobylitsa, Phys. Rev. D 65 (2002) 077504.
[58] W. Broniowski, E. Ruiz Arriola, K. Golec-Biernat, Phys. Rev. D 77 (2008) 034023, arXiv:0712.1012 [hep-ph].